Geomech. Geophys. Geo-energ. Geo-resour. (2018) 4:175–192
https://doi.org/10.1007/s40948-018-0082-x

ORIGINAL ARTICLE

Failure response of composite rock-coal samples

Hongwei Zhang · Derek Elsworth · Zhijun Wan

Received: 7 October 2017 / Accepted: 17 January 2018 / Published online: 29 January 2018
© Springer International Publishing AG, part of Springer Nature 2018

Abstract To accurately predict coal burst hazards and estimate the failure of coal pillars in underground coal mining systems, it is of great significance to understand the static and dynamic mechanical behavior of rock-coal structures. In experimental scale modeling, rock-coal structures are usually considered as samples (typically φ50 mm $\times$ 100 mm) composed of rock or coal components. This work examines the coupled effects of height ratio (a ratio of the height of coal to the height of whole sample) and loading rate on the mechanical interactions of composite samples using granular dynamic models. Results show that: (1) The peak strength of the composite sample decreases with increasing height ratio, while the peak strength increases linearly with loading rate under uniaxial compression. (2) Both the height ratio and loading rate have a significant effect on the micro-cracking in the composite sample. Micro-cracking evolves with strain and this rate increases first slowly and then advances rapidly. (3) Composite samples fail in a progressive manner, and the failure of the coal components controls the collapse of the ensemble sample. Specifically, cracks develop preferentially in the coal and then propagate into the rock.

Keywords Composite sample · Failure mode · Height ratio · Loading rate · Peak strength · Rock burst

1 Introduction

Rock and coal burst hazards and failure of coal pillars are experienced in underground mining, causing both injury and damage to facilities. Rock-coal pillar bursts refer to a violent failure of rock-coal structures and have been a major safety concern in underground longwall mining and room-pillar mining systems (Fig. 1a) (Dou et al. 2012; Kidybiński 1981; Mazaira and Konicek 2015; Salamon et al. 2003; Wang et al. 2006, 2017; Zhang et al. 2016). These pillars, composed of rock and coal (Fig. 1b, c), are frequently formed and retained to support the overlying strata and protect the mining space. Therefore, understanding the mechanical interactions between rock strata and coal seams are vital to retain the stability of pillars and the safety of mining activities (Shabanimashcool and Li 2012; Singh et al. 2011; Wagner 1980; Zhang et al. 2013).

H. Zhang · Z. Wan (✉)
Key Laboratory of Deep Coal Resource Mining (CUMT), Ministry of Education of China, School of Mines, China University of Mining & Technology, Xuzhou 221116, China
e-mail: zhjwan@126.com

H. Zhang · D. Elsworth
Department of Energy and Mineral Engineering, G3 Center and EMS Energy Institute, The Pennsylvania State University, University Park, State College, PA 16802, USA

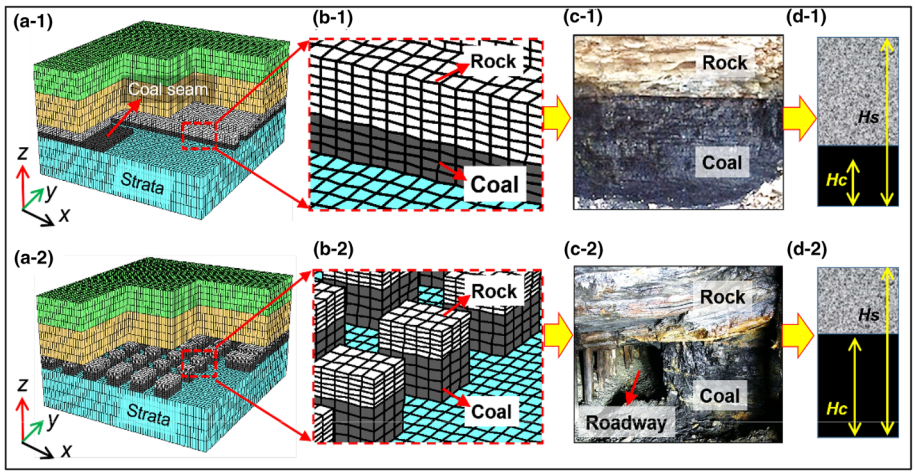

Fig. 1 Two typical underground coal mining systems, coal-rock combinations, and samples composed of rock and coal. **a-1**, **a-2** are 3D schematics of underground longwall mining and room-pillar mining systems, respectively. **b-1**, **b-2** are two kinds of pillars composed of rock and coal. **c-1**, **c-2** are in situ coal-rock combinations. **d-1**, **d-2** are schematics of simplified composed samples with different height ratios

To investigate the mechanical properties and failure behavior of coal pillars, pure coal and/or pure rock samples may be used (Bieniawski 1968; Hoek and Brown 1997; Medhurst and Brown 1998; Wang et al. 2013; Zhang et al. 2017). The main drawback is that pure samples cannot accurately reflect the overall mechanical properties of composite rock-coal structures. Therefore, the use of samples composed of rock and coal components should also be considered.

In underground mining, the failure of such composite pillars is influenced by several factors, such as the composite type determined by geometric dimensions of different strata, and the loading rate caused by different mining speeds (Huang and Liu 2013). Thus, the coupled effects of composition and loading rate on samples is important. In this work, the composition is represented by the height ratio (R) which is a ratio of the height of coal (H_c) to the height of sample (H_s) (i.e., $R = H_c/H_s$, Fig. 1d).

To date, compression tests on composite samples have been extensively conducted (as shown in Table 1), however, coupled effects of height ratio and loading rate on the failure behavior of composite samples are rarely available. In terms of mechanical behavior, the mechanical properties of a composite sample depend principally on the coal component (Liu et al. 2015). In addition, the height ratio and loading rate have a significant effect on the mechanical properties of composite samples. Dou et al. (2006) found that composite samples with a lower height ratio tends to burst easier than homogeneous samples. Chen et al. (2017) reported that the peak strength of composite sample decreases with increasing height ratio. By studying the influence of loading rate on mechanical behavior of composite samples, both Huang and Liu (2013) and Dou et al. (2006) indicated that the peak strength of composite samples increased linearly with loading rate, which is similar to binary geomaterials (Bieniawski 1968; Lankford 2010; Olsson 1991; Sano et al. 1981).

Besides mechanical behavior, deformation behavior of composite samples under uniaxial tests was also studied. Zuo et al. (2011) and Liu et al. (2015) indicated that the coal components experienced splitting failure, although the composite sample demonstrated conjugate X-shaped shear failure. Zhao et al. (2016) identified a partial failure in the coal component along a shear band with an inverted "V" shape. Chen et al. (2017) revealed that the coal component could be crushed with low height ratios, and the failure types of the rock sections could all be different—including splitting, shear or undamaged modes.

These previous results contribute to our knowledge of the mechanical and failure behavior of composite samples. The majority of previous results focused on a specific height ratio between 0.1 and 0.6, which is difficult to understand the progressive failure of rock-coal structures. Furthermore, pillars are various in

Table 1 Research on different composed samples in compression tests

Type	Materials	Loading rate	Height ratio	Size (mm)	Testing method	References
R–R	Granite, marble and Vicenza stone	–	0.5	–	Uniaxial	Greco et al. (1993)
R–C	Sandstone and coal	–	0.23	$\varphi 50 \times 100$	Uniaxial	Dou et al. (2006)
R–C	Sandstone and coal	–	0.6	$\varphi 50 \times 100$	Uniaxial	Dou et al. (2006)
R–C	Sandstone and coal	10^{-3} mm/s	0.5	$\varphi 35 \times 70$	Uniaxial and triaxial	Zuo et al. (2011)
R–C	Soft rock and coal	2×10^{-5} mm/step	0.5	$\varphi 50 \times 100$	Uniaxial and triaxial	Zhao et al. (2016)
R–C	Sandstone and coal	5×10^{-4} mm/s	0.1–0.5	$\varphi 50 \times 100$	Uniaxial	Chen et al. (2017)
R–C	Sandstone and coal	0.2 mm/min	0.5	$\varphi 50 \times 100$	Uniaxial	Zhao et al. (2010)
R–C–R	Sandstone, coal and mudstone	0.2 mm/min	0.33	$\varphi 50 \times 100$	Uniaxial	Zhao et al. (2010)
R–C–R	Sandstone and coal	0.2, 1, 3.25, 5.5, 7.75, 10, and 12.25 kN/s	0.2	$\varphi 50 \times 100$	Uniaxial	Huang and Liu (2013)
R–C–R	Limestone, coal and mudstone	300 N/s	0.4	$\varphi 50 \times 100$	Uniaxial	Liu et al. (2015)

Notice, 'R–R' represents a sample composed of two kinds of rocks. 'R–C' refers to a sample composed of rock and coal. In a 'R–C–R' sample, coal is sandwiched between rocks. '–' means the information was not mentioned

geometry, and rock bursts and pillar failures in underground coal mining are usually influenced by coupled stress conditions and rock-coal geometry. Therefore, factors such as height ratio, loading rate and material properties should be systematically considered in compression tests. In this study, we numerically simulate uniaxial compression tests on composite samples under various loading rates using the particle flow code (PFC).

2 Discrete element modeling

The particle flow code in two dimensions (PFC 2D) was used to model the physical tests (Potyondy 2007). This software employs a discrete element modeling (DEM) algorithm. The DEM method iteratively solves Newton's second law of motion for an assembly of particles with a pre-defined constitutive model applied at the grain–grain contacts. In the DEM modelling, calibration of the contact model is essential.

2.1 Parallel bond model (PBM) in PFC

There are two basic bond models in PFC. These are a contact bond model (CBM) and parallel bond model (PBM) (Cho et al. 2007). The CBM can only transmit forces acting at a contact point, while the PBM can transmit both forces and moments between particles. In PFC, the rock is represented as a heterogeneous material composed of cemented grains. The PBM provides the mechanical behavior of cemented contacting particles, and has been widely employed to estimate the mechanical behavior of rocks (Potyondy 2007; Potyondy and Cundall 2004; Yoon 2007). Therefore, in this work we chose the PBM to carry out the numerical simulation.

As shown in Fig. 2, the sample comprises numerous rigid particles which interact with each other at their parallel bond contacts. The parallel-bond components act in parallel with the linear components, and establish an elastic interaction between particles (Fig. 2c). The parallel bonds can also be envisioned as a set of elastic springs with normal and shear stiffness (K_n and K_s). These springs act together to model particle stiffness at a point. With these mechanical components, relative motion at the contact can cause a force and a moment to act on two bonded particles. If the given tensile or shear critical force at the bond is exceeded, failure of the bond occurs as representative of the initiation of a crack (Itasca 2014).

Notice that the in situ interface between rock and coal layers would influence the crack initiation and propagation during failure process. In this study, the interface between these two layers is considered as a layer of particles with different contact bonds. These

bonds, either contacted with rock or contacted with coal, are various in parameters (e.g. parallel bond tensile and shear strength). As shown in Fig. 2d, these particles at the interface were armed with different contacts in which some are contacts in rock and the remaining are contacts in coal.

2.2 Materials and numerical simulation design

2.2.1 Materials

Samples composed of sandstone and coal were employed to conduct uniaxial compression tests. The coal and sandstone were taken from the Yunhe coal mine (Jining, Shandong Province, China) (Chen et al. 2017). Compression tests were conducted on samples 50 mm in width and 100 mm in height (Bieniawski and Bernede 1979). In this study, 11 groups of standard specimens (φ50 × 100 mm) were tested (group numbers ranging from RC0 to RC10) by distributing different height ratios (R) ranging from 0 to 1.0 (Fig. 3). Each numerical sample was discretized into 6811 particles, and the particle size (i.e., diameter) followed a uniform distribution ranging from 0.35 to 0.58 mm. The average unit weights of sandstone and coal were 2600 and 1800 kg/m^3, respectively. Table 2 shows the physical and mechanical parameters of the sandstone and coal materials. The calibrated results are presented in Sect. 3, as comparisons between experimental and numerical data of intact and composite specimens under uniaxial compression.

2.2.2 Simulation procedures

In each group, 12 samples were generated to conduct uniaxial compression tests under various loading rates (i.e., 0.01, 0.03, 0.06, 0.09, 0.12, 0.15, 0.2, 0.3, 0.4, 0.5, 0.6, 0.7 m/s) (Table 3). In total, 121 composite samples were tested. During each compression test, an external axial displacement was applied to the top of the specimen. The test was terminated at 40% of the peak strength. In order to investigate the effects of loading rate and height ratio on the evolution of deformability of the samples, the evolution of the numbers of individual cracks (broken bonds) were used.

The numerical loading rate is related to time step, which is different from the loading rate employed in laboratory tests (Itasca 2014; Zhang and Wong 2014). The time step in each calculation cycle was 1.2 × 10^{-7} s. Thus, loading rates of 0.01 and 0.7 m/s can be translated to 1.2 × 10^{-6} and 8.4 × 10^{-5} mm/step, respectively. A 1.2 × 10^{-6} mm/step implies that

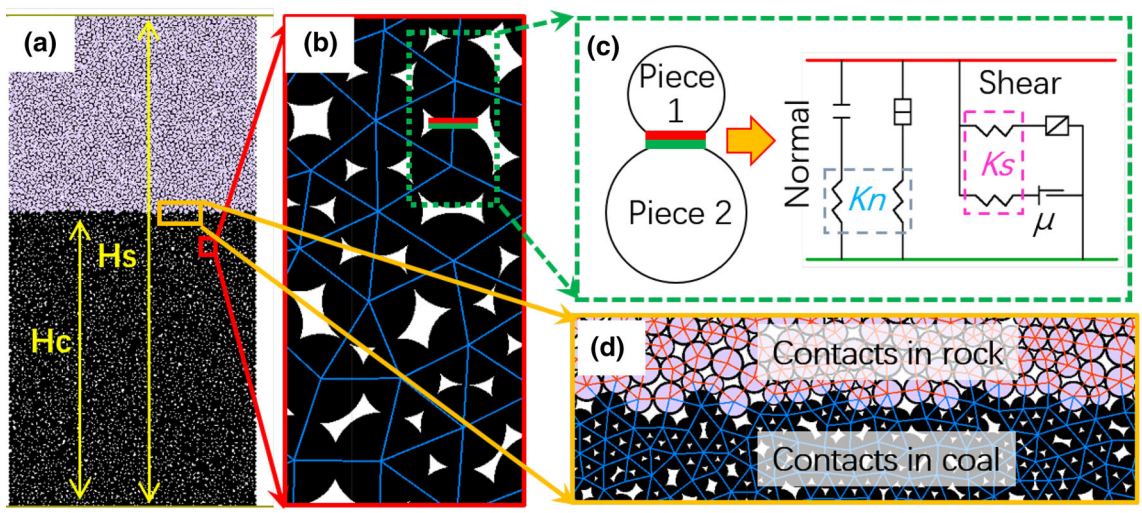

Fig. 2 Samples composed of coal and rock, and represented by the parallel bond model in PFC. **a** A typical composite sample (u50 × 100 mm) generated by PFC2D. The white and black particles are rock and coal materials, respectively. The height ratio ($R = H_c/H_s$) is a ratio of the coal height (H_c) to sample height (H_s). **b** Particles with pre-defined parallel bonds. **c** Components of the parallel bond model. K_n and K_s are normal and shear stiffness, respectively. μ is the friction coefficient (Itasca 2014). **d** Bonds are shown in red and blue lines indicating contacts in rock and coal, respectively

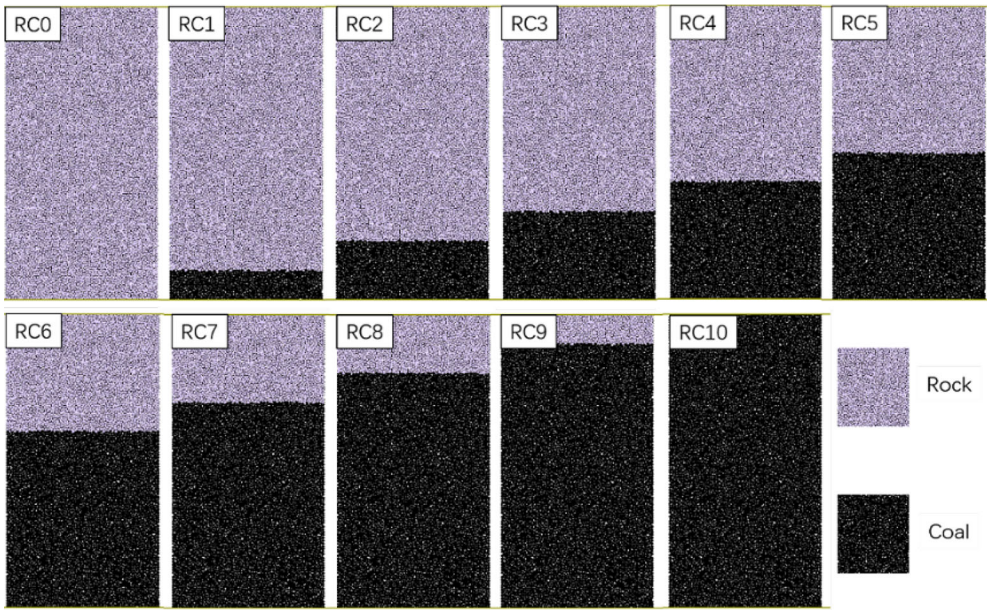

Fig. 3 Numerical samples with various height ratios ranging from 0 to 1.0. (RC0–RC10 represent group numbers)

Table 2 Physical and mechanical parameters used in the numerical simulations

Category	Sandstone	Coal	Unit
Density	2600	1800	kg/m^3
Radius	0.35–0.58	0.35–0.58	mm
Parallel-bond tensile strength	24.0	40.0	MPa
Parallel-bond cohesive strength	8.4	15.0	MPa
Inter-particle Friction	0.577	0.577	N/A
Effective Modulus	4.30	1.69	GPa
Normal-to-shear Stiffness Ratio	2.5	2.5	N/A

it requires more than 830,000 steps to move the loading plate 1.0 mm.

3 Calibrated parameters by experimental results of pure and composed samples

3.1 Calibrated results of pure sandstone and pure coal samples

Figure 4 shows the numerical stress–strain curves of pure sandstone and pure coal samples under uniaxial compression. The elastic deformation behavior and stress drop stages are well illustrated. Both the coal and sandstone samples are brittle materials, as apparent from the sudden stress drops post-peak strength. The peak strength, σ_p, is equivalent to the uniaxial compressive strength, and the elastic modulus, E, refers to the slope of the linear part of a stress–strain curve.

Calibration of the contact model is required in the DEM modeling. This is achieved by comparing modeling and experimental data. Table 4 shows the comparison results between experimental and numerical data of pure sandstone and pure coal samples. The numerical peak strengths of pure sandstone and pure coal samples are consistent with the experimental data: 88.90 versus 87.30 MPa, and 30.60 versus 29.24 MPa, respectively. In accordance with the comparison results, it can be concluded that the parameters listed in Table 2 are suitable to represent the mechanical properties of the sandstone and coal materials.

Table 3 Simulation design and numerical test conditions

Group numbers	RC0	RC1	RC2	RC3	RC4	RC5	RC6	RC7	RC8	RC9	RC10
Height of coal body (mm)	0	10	20	30	40	50	60	70	80	90	100
Height of sample (mm)	100	100	100	100	100	100	100	100	100	100	100
Height ratio	0	0.1	0.2	0.3	0.4	0.5	0.6	0.7	0.8	0.9	1.0
Sample number	12	12	12	12	12	12	12	12	12	12	12
Loading rate (m/s)	0.01, 0.03, 0.06, 0.09, 0.12, 0.15, 0.2, 0.3, 0.4, 0.5, 0.6, 0.7										

3.2 Calibrated results of composite samples

Figure 5 shows the comparisons between experimental and numerical parameters of the composite samples with height ratios of 0.1, 0.2, 0.3, 0.4 and 0.5. It is clear that the numerical stress–strain curves are in good agreement with the experimental data, including the stage of elastic deformation, the stage of crack initiation and the stage of failure. However, due to the closure of primary cracks, pores and voids in the real sandstone and coal (Yang et al. 2014), the experimental curves show an upwards concave trend at low stress levels—representing seating-in of the particle bonds.

In accordance with Fig. 5, Table 5 presents the calibrated results in detail. The numerical peak strengths of the composite samples with height ratios of 0.1, 0.2, 0.3 and 0.4 agree well with the experimental strengths. However, the experimental peak strength of samples with a height ratio of 0.5 are lower than that of the numerical data—this may be caused by natural flaws in the physical coal specimen, and the flaws play an important role in reducing coal strength (Hoek and Brown 1997).

4 Results and discussion

4.1 Effects of height ratio on stress–strain curves and peak strengths of composed samples

4.1.1 Effect of height ratio on stress–strain curves

Typical stress–strain curves of samples under various height ratios and loading rates are shown in Fig. 6. It is clear that the height ratio and loading rate exert a key effect on the mechanical and deformation behavior of the composite samples.

In general, two typical stages can be identified in these stress–strain curves—namely elastic deformation followed by post-peak strength response. During elastic deformation, the loading increases linearly with axial strain and elastic deformation dominates the stress–strain response of the composite samples. The

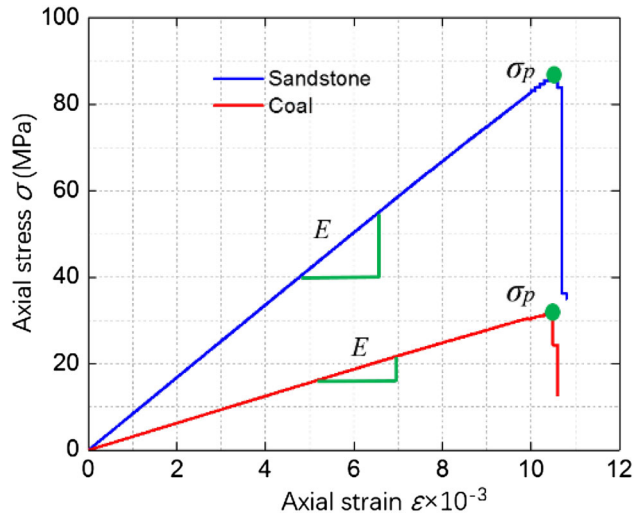

Fig. 4 Numerical stress–strain curves for pure sandstone and pure coal samples

Table 4 Calibrated peak strengths and elastic modulus for sandstone and coal specimens (Chen et al. 2017)

Rock type	Peak strength (MPa)		Elastic modulus (GPa)	
	Experimental	Numerical	Experimental	Numerical
Sandstone	87.30	88.90	8.13	8.25
Coal	29.24	30.60	3.06	3.04

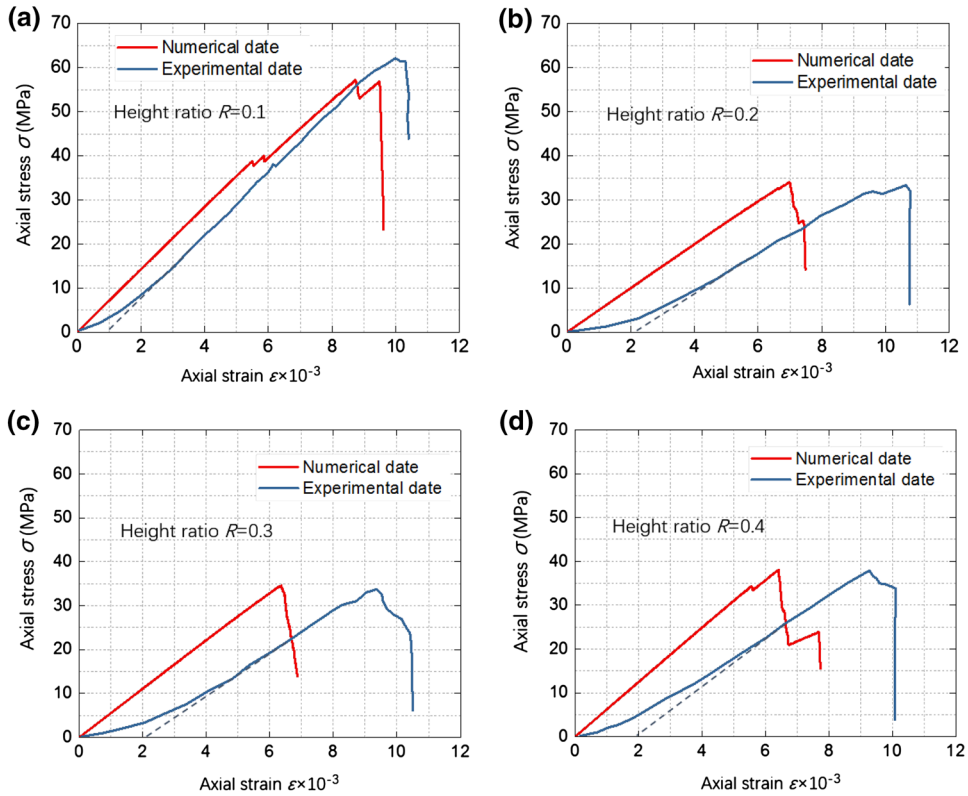

Fig. 5 Comparison between experimental and numerical stress–strain curves of composite samples under uniaxial compression. The experimental curves of composite samples are obtained from Chen et al. (2017)

linear stress–strain behavior does not change, although there are some irreversible processes, such as crack initiation (see the red line in Fig. 6a). At the conclusion of elastic deformation, the peak strength is exceeded and unloading initiates. A sudden stress drop occurs and identifies the post-peak stage—congruent with the generation and coalescence of micro-fractures. For samples compressed at a specific loading rate, such as the curves shown in Fig. 6a, the shapes of the stress–strain curves are consistent. However, for samples under different loading rates, the stress–strain curves vary in shape, especially the post-peak stages (as discussed in Sect. 4.2).

In addition to the shape of the stress–strain curve, the evolution of the mechanical properties can also be identified. The peak strength decreases with an increase in the height ratio (Fig. 6). Where only a slight decrease occurs, the majority of peak strengths are of the order of * 30 MPa—close to the peak strength of pure coal. The peak strain (corresponding to peak strength) can be divided into two stages, i.e., a decreasing and an increasing stage. As shown in

Table 5 Comparison between experimental and numerical parameters of composed samples

Group	Height ratio	Peak strength (MPa)		Elastic modulus (GPa)	
		Experimental	Numerical	Experimental	Numerical
RC1	0.1	62.09	57.10	7.03	6.55
RC2	0.2	40.00	38.00	3.16	5.94
RC3	0.3	36.14	34.50	4.57	5.47
RC4	0.4	41.64	34.10	4.53	4.89
RC5	0.5	17.99	33.10	3.05	4.44

Fig. 6, the peak strain initially decreases with increasing height ratio and then rises with height ratio. This may result from the difference in stiffnesses within the sample.

4.1.2 Relation between height ratio and peak strength

Figure 7 presents the relation between height ratio (R) and peak strength (σ_p) (namely R–σ_p relationship). The peak strength decreases with increasing height ratio but this change reduces with increased height ratio. In the R–σ_p curve (Fig. 7), a critical point divides the curve into two stages. Prior to the critical height ratio, the peak strength decreases sharply with increasing height ratio, with only a slight drop identified afterwards.

Interestingly, the critical height ratios vary for samples under different loading rates. Generally, the critical height ratio increases with increasing loading rate. According to the values of the critical height ratios, we divide the R–r_p curves into four groups in the ranges 0.01–0.09, 0.12–0.20, 0.30–0.50 and

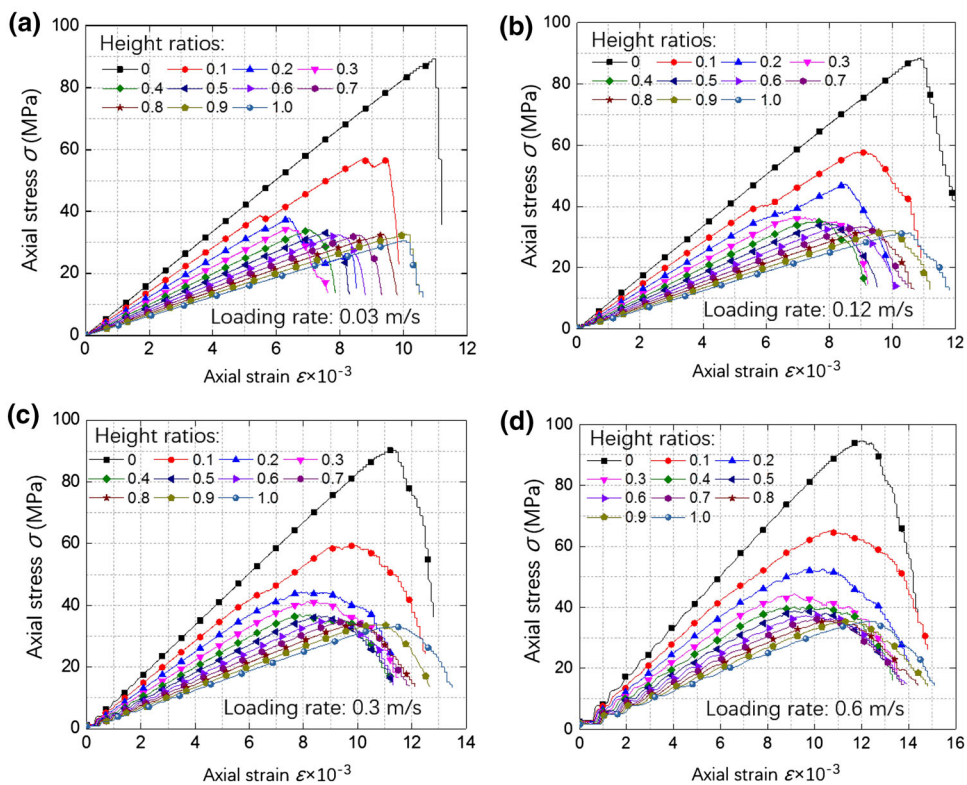

Fig. 6 Typical stress–strain curves under various height ratios and loading rates. **a** Stress–strain curves under loading rates of 0.03 m/s. **b** Stress–strain curves under loading rates of 0.12 m/s. **c** Stress–strain curves under loading rates of 0.30 m/s. **d** Stress–strain curves under loading rates of 0.60 m/s

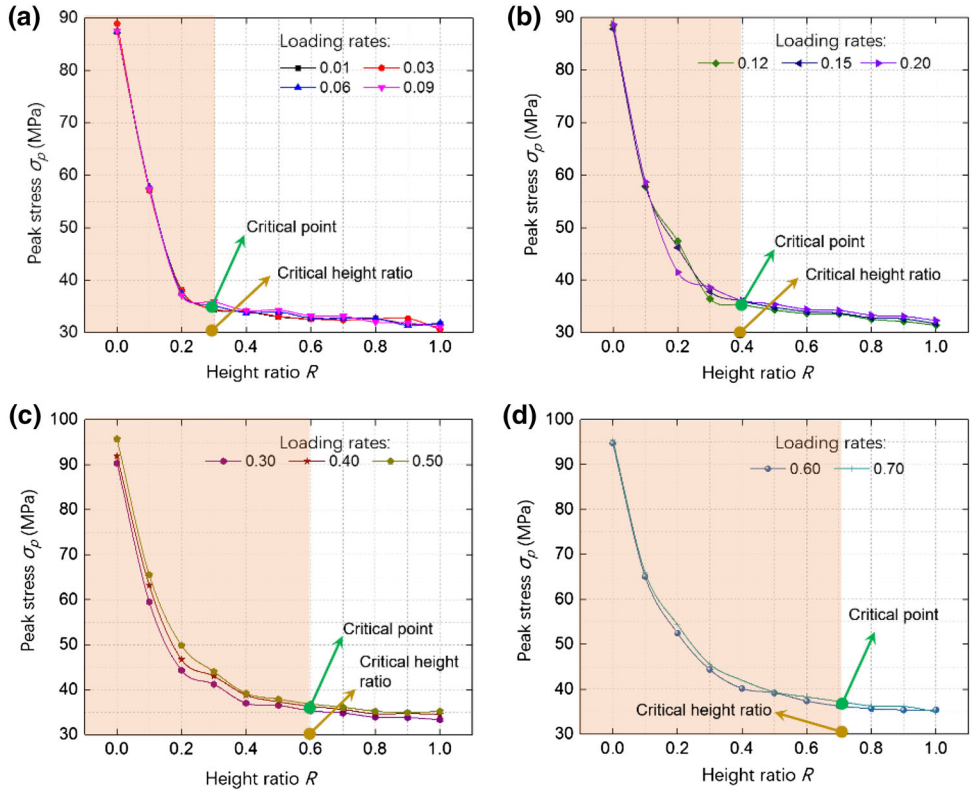

Fig. 7 Effect of height ratio on peak strength. **a** Peak strength versus height ratio for loading rates of 0.01, 0.03, 0.06 and 0.09. **b** Peak strength versus height ratio curves for loading rates of 0.12, 0.15 and 0.20. **c** Peak strength versus height ratio curves for loading rates of 0.30, 0.40

0.60–0.70 m/s (as shown in Fig. 7). Further, the critical ratios can be identified as 0.3, 0.4, 0.6 and 0.7 for these groups, respectively. The R–σ_p curves in the group for 0.01–0.09 m/s (Fig. 7a) and the group for 0.60–70 m/s (Fig. 7d) appear independent of loading rate. This implies that loading rates between 0.01 and 0.09 m/s are sufficiently low (quasi-static), and that loading rates between 0.6 and 0.7 m/s are sufficiently high that no rate effects are apparent. This phenomenon is in turn confirmed from the numerical models investigating the influence of loading rate on the mechanical properties of samples.

To present the R–σ_p relationship in a direct manner, we define a modified peak strength (σ_p') equal to the peak strength (σ_p) multiplied by the height ratio (R). This is defined as:

$$\sigma_p' = \sigma_p \times R \tag{1}$$

where σ_p' is the modified peak strength, MPa; σ_p is peak strength, MPa, and R is height ratio.

The modified peak strength (σ_p') versus height ratio (R) curves (i.e., σ_p'–R curves) are shown in Fig. 8. A linear fit to the curves and their regression are also presented in Fig. 8 and Table 6, respectively. The values of peak strengths are detailed in Table 7.

As shown in Fig. 8, the modified peak strength (σ_p') increases linearly with increasing height ratio, and all right correlation coefficients are greater than 0.996—implying a high correlation. Therefore, the relation between the peak strength and height ratio can be described by an inversely proportional function and expressed as:

$$\sigma_p = \sigma_n + m=R \tag{2}$$

where σ_n and m are parameters recovered from the regression functions.

As previously mentioned many studies have investigated the mechanical behavior of composite samples—typically with height ratios of the order of 0.5. However, the height ratio of 0.5 is located in the

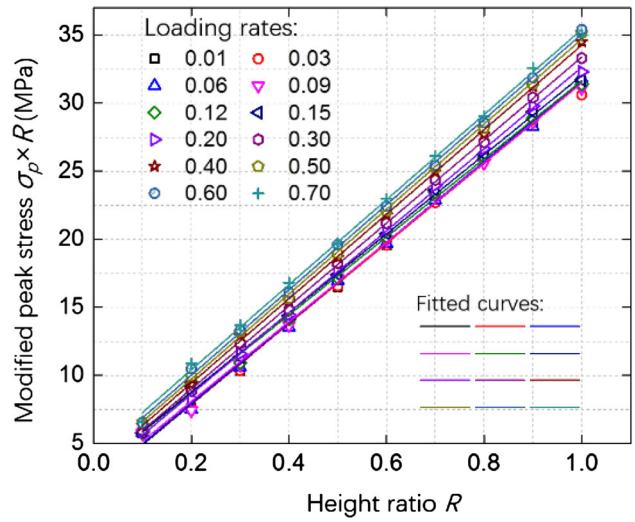

Fig. 8 Modified peak strength versus height ratio curves

Table 6 Regression results of σ_p'–R and σ_p–R relations

Loading rate	σ_p'–R relationship	σ_p–R relationship	Correlation coefficients
0.01	$\sigma_p \times R = 29.64R + 1.94$	$\sigma_p = 29.64 + 1.94/R$	0.998
0.03	$\sigma_p \times R = 29.43R + 2.03$	$\sigma_p = 29.43 + 2.03/R$	0.996
0.06	$\sigma_p \times R = 29.60R + 2.03$	$\sigma_p = 29.60 + 2.03/R$	0.998
0.09	$\sigma_p \times R = 29.21R + 2.25$	$\sigma_p = 29.21 + 2.25/R$	0.998
0.12	$\sigma_p \times R = 28.66R + 2.97$	$\sigma_p = 28.66 + 2.97/R$	0.998
0.15	$\sigma_p \times R = 29.03R + 2.98$	$\sigma_p = 29.03 + 2.98/R$	0.999
0.20	$\sigma_p \times R = 30.00R + 2.62$	$\sigma_p = 30.00 + 2.62/R$	0.999
0.30	$\sigma_p \times R = 30.45R + 2.91$	$\sigma_p = 30.45 + 2.91/R$	1.000
0.40	$\sigma_p \times R = 31.04R + 3.21$	$\sigma_p = 31.04 + 3.21/R$	0.999
0.50	$\sigma_p \times R = 31.19R + 3.49$	$\sigma_p = 31.19 + 3.49/R$	0.999
0.60	$\sigma_p \times R = 31.31R + 3.74$	$\sigma_p = 31.31 + 3.74/R$	0.999
0.70	$\sigma_p \times R = 31.24R + 4.15$	$\sigma_p = 31.24 + 4.15/R$	0.999

transitory portion of the R–r_p curve, where the loading behavior of the rock-coal structure is similar to that of pure coal. Only testing a composite sample with specific height ratios spanning this threshold allows an understanding of behavior–as completed here. This R–r_p relationship also focuses attention on the mechanical interactions between rock and coal as composite structures when estimating the stability of composite coal pillars.

4.2 Effects of loading rate on stress–strain curves and peak strengths

4.2.1 Effect of loading rate on stress–strain curves

Numerical stress–strain curves for eight loading rates of 0.001, 0.12, 0.2, 0.3, 0.4, 0.5, 0.6 and 0.7 m/s are presented in Fig. 9. It can be seen that the loading rate has a significant influence on the post-peak response, while the elastic deformation is largely independent of loading rate.

The peak strength and peak strain of samples rises with increasing loading rate. After peak strengths are exceeded, the stress–strain curves drop in different manners. Specifically, a faster loading rate results in

Table 7 Peak strengths under various height ratios and loading rates

Height ratio (R)	Peak strengths (σ_p) under various loading rates (MPa)											
	Loading rate (m/s)											
	0.01	0.03	0.06	0.09	0.12	0.15	0.2	0.3	0.4	0.5	0.6	0.7
Peak strength (MPa)												
0	87.4	88.9	87.5	87.5	88.5	87.8	88.7	90.3	91.9	95.7	94.7	95.6
0.1	57.2	57.1	57.8	57.4	57.8	57.9	58.7	59.5	63.2	65.5	65.1	66.0
0.2	38.1	38.0	37.5	37.1	47.4	46.2	41.5	44.3	46.7	49.8	52.5	54.4
0.3	34.4	34.5	35.2	35.9	36.4	37.8	38.6	41.2	43.0	44.0	44.4	45.6
0.4	34.0	34.1	33.8	34.2	35.3	36.0	36.1	37.0	38.8	39.2	40.2	42.0
0.5	33.0	33.1	33.9	34.3	34.3	34.8	35.4	36.5	37.3	37.9	39.2	39.4
0.6	32.6	32.6	32.8	33.2	33.6	34.0	34.4	35.3	36.3	36.8	37.4	38.3
0.7	32.7	32.4	32.7	33.1	33.5	33.7	34.2	34.8	35.6	36.1	36.3	37.3
0.8	32.6	32.6	32.7	32.0	32.5	32.8	33.3	33.9	34.6	35.2	35.7	36.3
0.9	31.7	32.7	31.4	31.8	32.1	32.6	33.1	33.8	34.7	34.9	35.4	36.2
1.0	31.6	30.6	31.8	31.1	31.4	31.7	32.3	33.3	34.5	35.2	35.4	35.0

more obvious strain softening behavior. That is, the slope of the post-peak curve becomes more shallow with an increase in loading rate. This phenomenon indicates that the growth in the loading rate increases the ductility of composite sample at the post-peak stage. This is consistent with prior conclusions (Jackson et al. 2008; Zhang and Wong 2014). The relation between loading rate and peak strength will be explored in detail in the following sections.

4.2.2 Relation between loading rate (v) and peak strength (σ_p)

Figure 10a illustrates the relation between loading rate and peak strength of composite samples (namely v–σ_p relationship). The peak strength rises linearly with increasing loading rate and is consistent with previous studies (Bieniawski 1968; Huang and Liu 2013; Lankford 2010; Olsson 1991; Sano et al. 1981). The regression functions and correlation coefficients are presented in detail in Table 8. The majority of the correlation coefficients are greater than 0.90, suggesting high correlation and reliability.

However, the linear v–σ_p curves vary amongst height ratios. Specifically, slopes of the fitted curves are different, and the slope for specimens with a height ratio of 0.2 is the greatest. To quantitatively identify the coupled effects of loading rate and height ratio on peak strength, we defined the incremental percentage ($D\sigma$) of peak strength, which can be expressed as:

$$D\sigma = (\sigma_{0:7} - \sigma_{0:01})/\sigma_{0:01} \times 100\% \quad (3)$$

where $D\sigma$ is the incremental percentage of the peak strength; $\sigma_{0.01}$ and $\sigma_{0.7}$ are peak strengths under loading rates of 0.01 and 0.70 m/s, respectively.

According to Eq. (3), the relation between height ratio and the incremental percentage of peak strength can be plotted as in Fig. 10b. All peak strengths were enhanced by 9.4–42.8% with an increase in loading rate from 0.001 to 0.70 m/s. However, the increment of peak strength varies with height ratio. Prior to the critical height ratio ($R = 0.2$), the incremental percentage increases rapidly from 9.4 to 42.8%. Beyond that, the incremental percentage decreases from 42.8 to 10.8%. A higher incremental percentage of peak strength implies a more stable response of composite sample when undergoing dynamic loading. Therefore, dynamic loading has proportionately less influence on the composite sample with a height ratio of 0.2.

In underground coal mining systems, the coal seam is sandwiched between the roof and floor strata. Some factors, for example dynamic loading, will surely intensify the failure and propensity for bursting of rock or coal (Bai et al. 2015; Huang and Liu 2013; Singh et al. 2011; Wagner 1980; Zhang et al. 2013, 2016). In accordance with the $D\sigma$–R curves shown in Fig. 10b, rock-coal structures with height ratios between 0.1 and 0.6 seem more stable when undergoing dynamic loading, in which the structure with a height ratio of 0.2 is the most prominent. That is probably because the

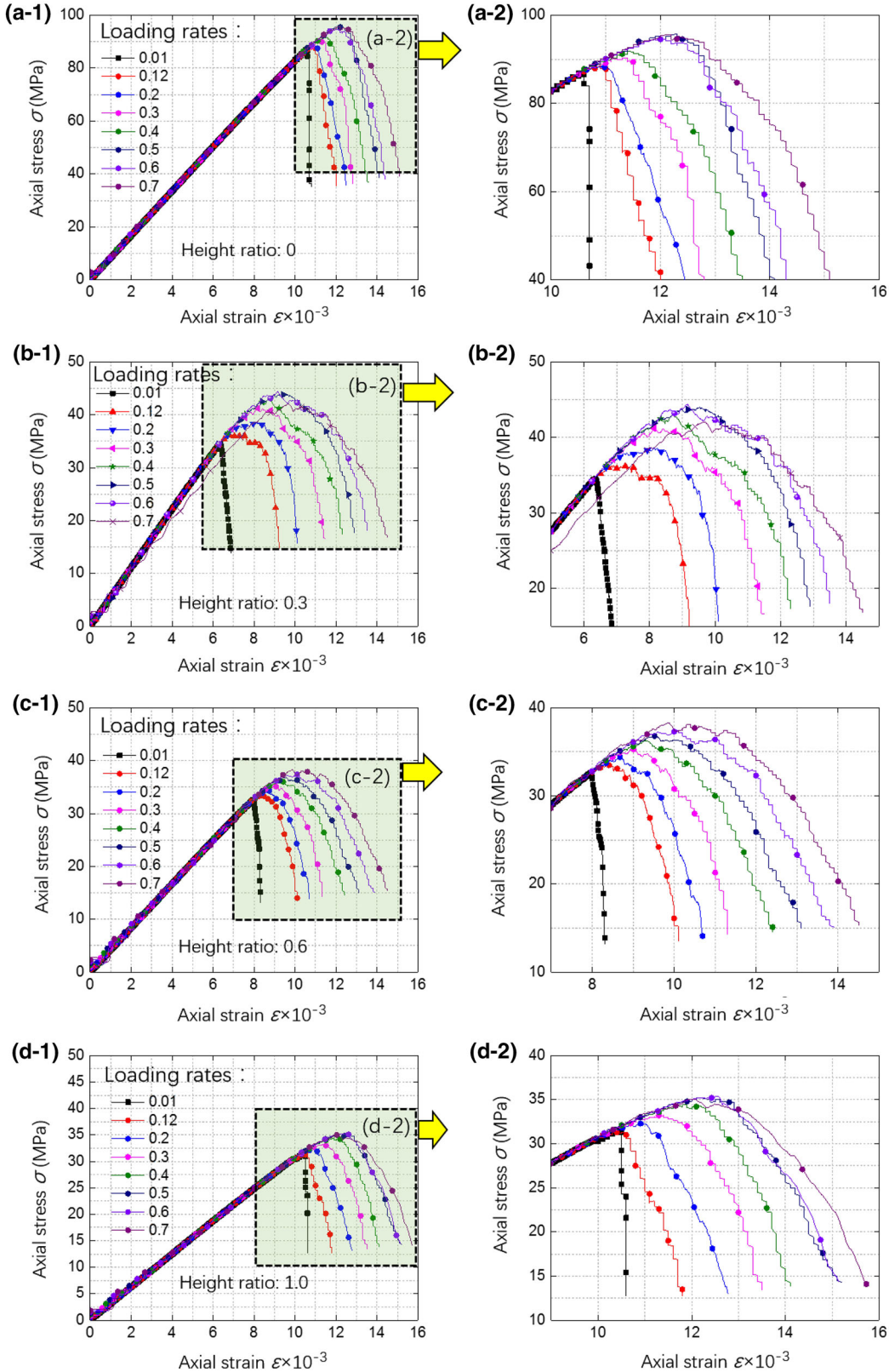
(a-1)
Loading rates：
0.01
0.12
0.2
0.3
0.4
0.5
0.6
0.7
(a-2)
Height ratio: 0
Axial stress σ (MPa)
Axial strain ε×10⁻³
(a-2)
(b-1)
Loading rates：
(b-2)
Height ratio: 0.3
(b-2)
(c-1)
Loading rates：
(c-2)
Height ratio: 0.6
(c-2)
(d-1)
Loading rates：
(d-2)
Height ratio: 1.0
(d-2)

b **Fig. 9** Effect of loading rate on stress–strain curves of samples. **a-1**, **a-2** Stress–strain curves of samples with a height ratio of 0. **b-1**, **b-2** Stress–strain curves of samples with a height ratio of 0.3. **c-1**, **c-2** Stress–strain curves of samples with a height ratio of 0.6. **d-1**, **d-2** Stress–strain curves of samples with a height ratio of 1.0

control on the failure of composite specimens transfers from the failure of rock component to the failure of coal at the height ratio of 0.2, thus leading to the anomalous relation. This transition will be analyzed in the next section (Sect. 4.4) which discusses the coupled effects of loading rate and height ratio on the failure modes of composite specimens. Therefore, the dynamic bearing capacity of rock-coal structures should be fully considered when estimating the tendency of rock/coal burst hazards and in designing the dimension of rock-coal pillars.

4.3 Coupled effects of height ratio and loading rate on micro-cracking activity

Evolution of micro-cracking is an important index to identify the deformation of specimens. In PFC2D, a micro-crack is initiated once a tensile or shear failure between two adjacent particles occurs (Itasca 2014). By monitoring the number of micro-cracks relative to evolving strain curves enables the effects of different loading rates to be examined (Fig. 11).

Two stages can be identified in the number-of-cracks versus strain curves (Fig. 11). Prior to the peak strain, the crack number grows only slowly with increasing axial strain. Subsequently, this number-of-cracks increases rapidly. In other words, the increasing rate of micro-crack formation is relatively low in the early stages of loading. After peak strain, the number of micro-cracks increases sharply due to the failure of the sample.

In the numerical simulations, compression was halted when a given strength (σ_r) was reached—at a σ_r of 40% of the peak strength (σ_p). Therefore, the total number of cracks is the number at the halted strength. At peak strengths, the numbers of cracks are all smaller than 1000—these low values indicate that the micro-cracks have initiated but have not yet extended to the full population at peak strength (Brady and Bray 1978). However, cracks always propagate at or beyond post-peak, thus, the majority of fracturing occurs after the peak. Unexpectedly, the micro-crack numbers at the halted strength increase almost linearly with increasing loading rate (see the red linear curves in the right portion of Fig. 11), suggesting that micro-cracking activity tends to be more intense under a higher loading rate.

4.4 Failure modes

4.4.1 Comparisons between experimental and numerical failure modes of composite samples

Figure 12 shows comparisons between experimental and numerical failure modes of composite samples with height ratios of 0.1, 0.2, 0.3, 0.4 and 0.5. Modes of failure for the numerical models are shown to the left with red dots representing individual micro-cracks

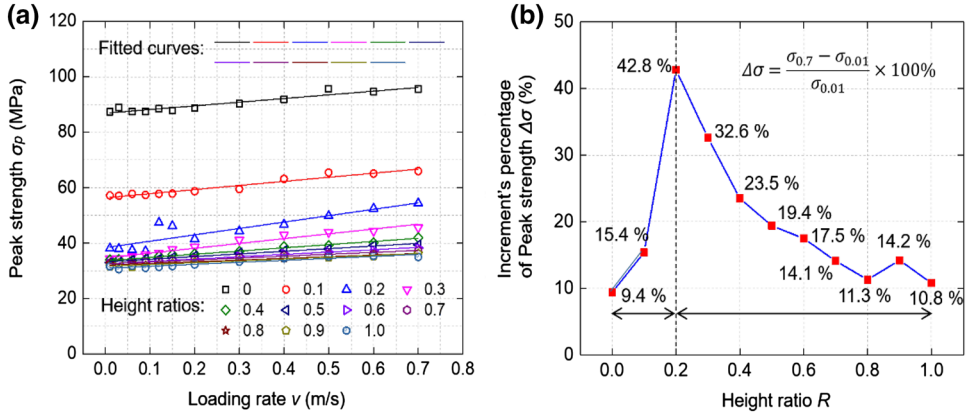

Fig. 10 Effects of loading rate and height ratio on peak strength of samples. **a** Relation between loading rate and peak strength. **b** Relation between height ratio and incremental percentage of the peak strength

(broken bonds). The results of laboratory experiments are shown to the right. The upper and lower are sandstone and coal components, respectively. It is clear that the numerical failure modes agree well with those observed in experimental modes. Clearly, the failure of the coal component is the dominant factor contributing to sample failures (Liu et al. 2015; Zhao et al. 2016; Zuo et al. 2011). In addition, micro-fracturing bands develop preferentially in the basal part of sample and propagate upwards towards the rock body. Thus, the failure of the sandstone component is caused by the punching of cracks from the coal into the sandstone. This is readily apparent in both numerical and experimental samples.

In accordance with the results compared in Fig. 12, the crack initiation and coalescence modes in the numerical experiments are in good agreement with those observed in the experiments. From the failed coal fragments shown in Fig. 12, it can be concluded that the brittle coal has a propensity to be pulverized—especially at small height ratios in the range 0.1–0.2 (i.e., RC1 and RC2). However, with increasing height ratio, the coal component tends to shear or split to columns.

4.4.2 Coupled effects of loading rate and height ratio on the failure modes of composite samples

Figure 13 illustrates the influences of loading rate and height ratio on the ultimate failure modes of samples under uniaxial compression. The majority of failures initiate in the coal components and these resulting shear bands can be readily identified in the coal. This failure mode is consistent with previous studies (Chen et al. 2017; Liu et al. 2015; Zhao et al. 2016; Zuo et al. 2011). However, the sandstone components tend to split axially, as seen clearly in samples with height ratios of the order of 0.1 and 0.2. The failure in the sandstone becomes more obvious for lower height ratios, of the order of 0.1–0.2. This is because the composite sample with a larger coal proportion cannot absorb more of the elastic energy applied by the compression.

Fig. 11 Number of micro-cracks versus axial strain curves. **a-c 1**, **a-2** are number of cracks versus strain for samples with a height ratio of 0. **b-1**, **b-2** are number of cracks versus strain for samples with a height ratio of 0.3. **c-1**, **c-2** are number of cracks versus strain for samples with a height ratio of 0.6. **d-1**, **d-2** are number of cracks versus strain for samples with a height ratio of 1.0

As shown in each row in Fig. 13, a higher loading rate always implies a much more severe failure of the sample resulting in a higher peak stress and larger post-failure deformation (Fig. 9). In addition, the shear fracturing bands develop preferentially in the bottom part of specimen (coal). As the loading rate increases, the development of cracks gradually extends to the upper portion. That is, a slow loading rate can limit the growth of cracks and shear bands, which has also been observed in other numerical studies (Shimizu et al. 2010; Zhang and Wong 2014).

In underground longwall and room-pillar mining systems, the failure of pillar would be in a progressive manner. The cracking bands would develop preferentially in the component of coal, then the development of cracks gradually extend to the roof. Furthermore, the determiner changes from rock to coal component

Table 8 Regressive functions of loading rate (v) and peak strength (σ_p)

Height ratio (R)	v–σ_p' relationship	Correlation coefficients
0	$\sigma_p = 13.25v + 86.88$	0.901
0.1	$\sigma_p = 14.78v + 56.38$	0.937
0.2	$\sigma_p = 23.03v + 38.39$	0.781
0.3	$\sigma_p = 17.40v + 34.67$	0.956
0.4	$\sigma_p = 11.55v + 33.68$	0.978
0.5	$\sigma_p = 9.52v + 33.25$	0.981
0.6	$\sigma_p = 8.47v + 33.55$	0.989
0.7	$\sigma_p = 6.88v + 32.56$	0.978
0.8	$\sigma_p = 5.97v + 32.11$	0.955
0.9	$\sigma_p = 6.61v + 31.63$	0.933
1.0	$\sigma_p = 7.12v + 30.95$	0.895

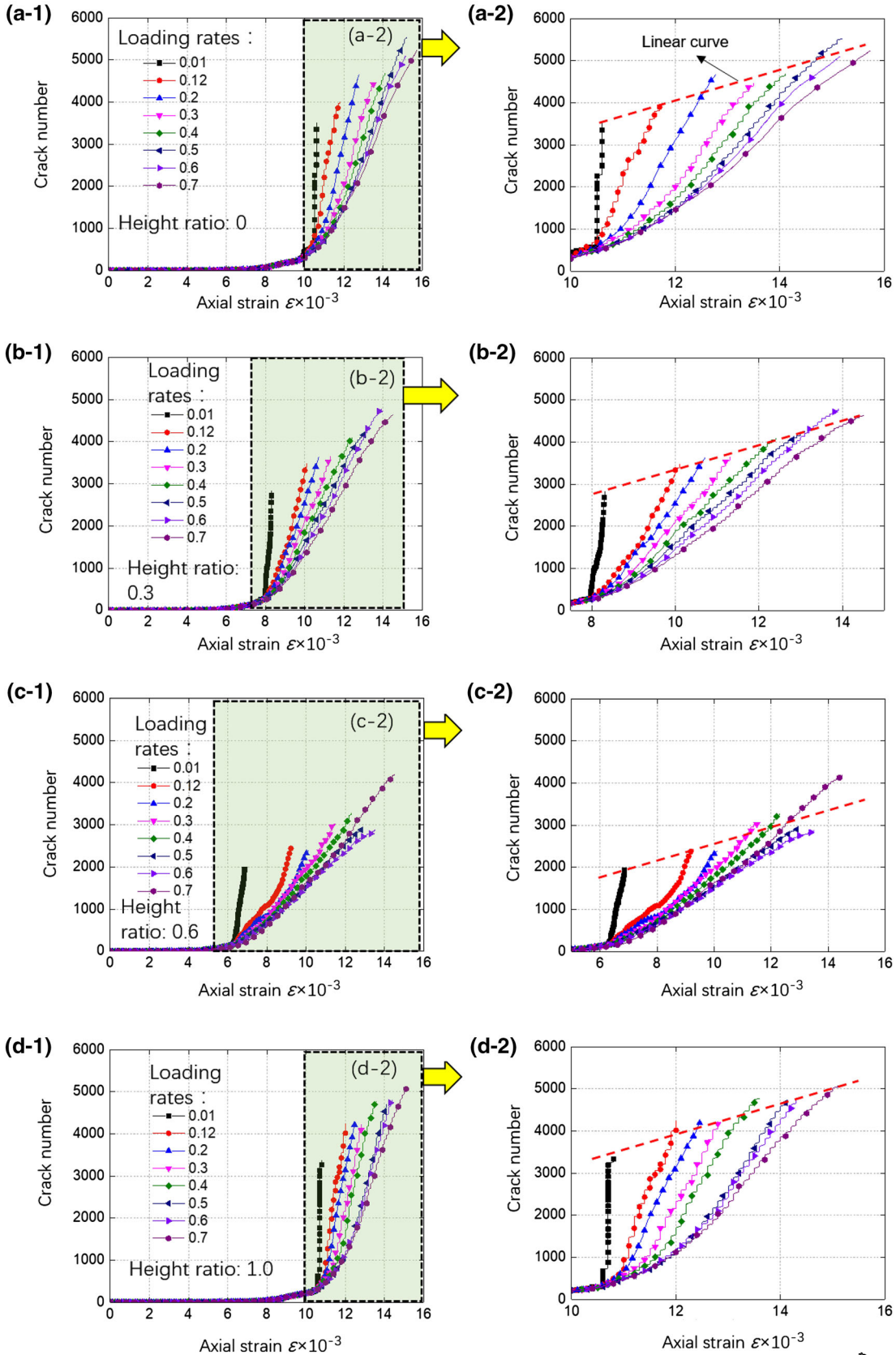
(a-1)
Loading rates :
0.01
0.12
0.2
0.3
0.4
0.5
0.6
0.7
Height ratio: 0
(a-2)
Linear curve
(b-1)
Loading rates :
Height ratio: 0.3
(b-2)
(c-1)
Loading rates :
Height ratio: 0.6
(c-2)
(d-1)
Loading rates :
Height ratio: 1.0
(d-2)
Crack number
Axial strain ε×10-3

Fig. 12 Comparison between experimental and numerical failure modes of samples under uniaxial compression

with the increasing height ratio (as shown in Figs. 7 and 13). Prior to the critical height ratio, the failure of pillar is determined by the failure of rock, while the failure is controlled by the failure of coal component afterwards. Therefore, the coal failure in the coal/roof structure with a height ratio lower than the critical height ratio may not result in the whole failure of rock-coal pillar. However, if the height ratio is greater than the critical value, the failure of coal would lead to failure of the whole structure. These results may contribute to predicting the hazards of coal bursts and estimating the failure of rock-coal structures in underground mining.

5 Conclusions

The effects of height ratio and loading rate are examined on the mechanical properties and failure behavior of composite specimens comprising layered assemblages of sandstone and coal. These behaviors are studied both experimentally and numerically with micro-models. Eleven groups of samples with various height ratios ranging from 0 to 1.0 were intensively tested under uniaxial compression conditions. Several important findings are apparent:

1. The peak strength of the composite samples decreases with increasing height ratio, but this